DIFFERENT STRATEGIES TO SIMULTANEOUSLY N-DOPING AND REDUCE GRAPHENE OXIDE FOR ELECTROCATALYTIC APPLICATIONS.

A. Romero[1]; M.P. Lavín-López[2]; A.R. de la Osa[1]; S. Ordoñez[1]; A, de Lucas-Consuegra[1]; J.L. Valverde[1]; A. Patón[1]

[1] *University of Castilla-La Mancha, Department of Chemical Engineering, Avenida Camilo Jose Cela 12, 13071, Ciudad Real (Spain).*

[2] *Graphenano S.L., Calle Pablo Casals 13, 30510, Yecla, Murcia (Spain).*

* Corresponding author e-mail: Antonio.Paton@uclm.es

Abstract

Two different approaches to simultaneously introduce nitrogen atoms within the graphene framework and, reduce graphene oxide nanoplatelets (GO), have been explored in order to improve the electrocatalytic activity of the resulting materials. Thus, a facile hydrothermal method using 2-chloroethylamine under conditions at 180 ºC and, another one, based in the formation of polypyrrole (PPy) on graphene oxide nanoplatelets by in situ polymerization of pyrrole monomer in the presence of GO, were compared through a deep characterization of the final materials by SEM, RAMAN, FTIR, XPS, Zeta potential, XRD and TGA analysis. Physico-chemical properties of the graphene-based materials were subsequently related with their electron transfer efficiency and electrocatalytic activity. The as prepared rGO prepared by the PPy method showed an N content quite superior (~6-8 %) than the rGO prepared by the hydrothermal one (~1%) being an important part of their nitrogen state pyridinic type. The electrocatalytic results showed that GO exhibited higher specific capacitance than rGO materials due to its intrinsic higher porosity. However, the presence of N species seems to have a positive effect on the ORR activity, although the N incorporation through the PPy-rGO synthesis method seems to be the preferred one according for the complete ORR pathway.

1. INTRODUCTION

Currently, it is of great significance to solve those problems associated to fuel cells (FC), a potential power source for vehicles and stationary applications, such as the oxygen reduction reaction (ORR) in the whole pH range at the cathode, which is responsible of a great cell voltage loss during the working operation [1]. Thus, one of the principal issues to make real the FC technology is the development of new and low-cost materials with elevated ORR activity.

Graphene-based materials such as graphene oxide (GO) prepared by oxidation of natural graphite and characterized by its high amount of oxygen containing functional groups on the surface, and specially, reduced graphene oxide (r-GO) produced using GO as precursor, are widely attended by their high catalytic activity and selectivity to H_2O_2 in alkaline or neutral medium for ORR [2, 3]. Thus, the carbon atoms neighboring to oxygen functional groups introduced in the graphite structure by oxidation, are considered active sites in which, intermediates absorption takes place accelerating the ORR. Moreover, N-doped graphene based materials prepared by different methods have demonstrated to be an efficient ORR electro-catalyst affecting the spin density and electron cloud distribution of neighboring C, inducing the formation of exceptional "active sites" [4, 5]. Among the three main chemical forms of N on the surface on N-doped graphene (pyridinic, pyrrolic and graphitic), some authors claim that graphitic-N is an energetic active site in which oxygen adsorption and then, ORR process takes place [6, 7, 8, 9]. Other authors have suggested that pyridinic-N also improve the chemisorption ability of oxygen functional groups of the carbon atoms near the pyridinic-N [10, 11] and others, that both N-types (pyridinic and graphitic) simultaneously influence ORR activity [12].

Different approaches have been used to introduce nitrogen atoms within the graphene structure being many of them highly complicated, difficult to scale and expensive [12]. N-doped graphene with low nitrogen concentration can be synthesized at large scale using hydrothermal procedures at low temperatures and, subsequent annealing [13, 14, 15]. On the other hand, a possible option to increase the N content onto the graphene oxide surface is based on the immobilization of an N-containing polymer forming a polymer/GO composite [16] which is then subjected to an annealing treatment. Thus, these N containing graphene including polymers are considered potential candidates to substitute Pt catalysts in ORR [17].

In this study, two different approaches to simultaneously introduce nitrogen atoms within the graphene framework and, reduce graphene oxide nanoplatelets, have been explored in order to improve the electrocatalytic activity of the resulting materials. Thus, a facile hydrothermal method using 2-chloroethylamine at 180 ºC and, another one, based in the formation of polypyrrole (PPy) on graphene oxide nanoplatelets by *in situ* polymerization of pyrrole monomer in the presence of GO, were compared through a deep characterization of the final materials. Physico-chemical properties of the graphene-based materials were subsequently related with their electron transfer efficiency and the electrocatalytic activity.

2. EXPERIMENTAL

2.1. Materials

Powder graphite (<20μm), 2-Chloroethylamine hydrochloride (99%), Ammonium persulfate (>98%), sodium hydroxide (>97%, pellets) and pyrrole (98%) were purchased from Sigma-Aldrich Chemistry®. Potassium permanganate (purity >99%), potassium chloride (99%), sulfuric acid (96%), hydrogen peroxide (110 vol.), HCl (5N) and ethanol (purity >99.5%) were purchase from Panreac®. HCl (purity >37%) was supplied by Honeywell and potassium hydroxide (>84%, pellets) by Merck.

2.2. Graphite oxidation.

Graphite oxidation was performed following the Improved Hummers Method using potassium permanganate ($KMnO_4$) as oxidizing agent. 15 g of graphite was dry mixed with 45 g of $KMnO_4$ (1:3). The mixture was slowly added to a vessel with sulfuric acid (H_2SO_4) and vigorously stirring for 3 hours at 50ºC. After that, the product obtained was mixed with 3 ml of H_2O_2 and ice in order to decrease the temperature generated for the exothermal reaction of H_2O_2 and the remaining $KMnO_4$. The brown mud produced after the mixture was vacuum filtered and washed with distilled water, chlorhydric acid and ethanol. After filtration, the remnant solid was dried at 60ºC during 2 hours With the aim of exfoliated graphene sheets, the powder was mixed with water and sonicated for 2 hours [18]. The obtained material was named as graphene oxide (GO).

2.3. Hydrothermal reduction of graphene oxide.

For the hydrothermal reduction, 6 g of GO was mixed with 19.5 g of 2-Chloroethylamine hydrochloride in distilled water (150 ml). The mixture was sonicated for 2 hours and stirring 2 more. Then, the solution was spilled onto an autoclave and heated to 180ºC (10ºC/min) for 12 hours. When the autoclave was cold, the product was filtered at vacuum and introduced into a quartz reactor under N_2 atmosphere. Thermal annealing was carried out in two steps: first step rising the temperature to 200ºC (5ºC/min) for 1 hour, and a second step rising the temperature to 450ºC (5ºC/min) for 3 hours. After that, the reactor was cooled down till room temperature. After that, the powder was washing with distilled water till the pH reach 7 and vacuum dried at 70 degrees for 6 hours [19]. The obtained material was named as HT-rGO.

2.4. Polypyrrole-reduced graphene oxide composite.

A bulk solution of 1g/L distillated water and graphite oxide was sonicated for 2 hours. After sonication, 4 ml of pyrrol was added to the dispersion and sonicated 5 minutes more and stirred for 10 minutes. During the stirring, ammonium persulfate (APS) solution was performed mixing 800 ml of distilled water and 2.12 g of APS This mixture was added slowly to the pyrrol/graphite oxide dispersion and stirred for 5 hours. Next, the dispersion was vacuum filtered and washed with ethanol and distillated water (400 ml). The obtained solid was overnight vacuum dried at 60ºC and 0.6MPa. Thermal annealing was carried out onto a quartz reactor. The dried powder was placed into in a N_2 atmosphere. The target temperature (450ºC, 700ºC) was maintained for 2 hours [20]. The obtained material was named as rGO-PPy*450* or rGO-PPy*700.*

2.5. Characterization of carbonaceous materials

X-Ray photoelectron spectroscopy (XPS) was performed by SPECS mod. PHOIBOS 150 MCD which use an X-ray source with Mg and Al anodes, monochromatic resource of Ag and Ar^+ ion cannon for the depth profile measure. Fourier transform infrared (FTIR) analysis was carried out on a SPECTRUM TWO spectrometer (Perkin Elmer, Inc) and performed in transmission mode using KBr (350-8300 cm-1) pellets and, ZnSe (550-6000 cm-1).Thermogravimetric analysis data were collected on a METTLER TOLEDO TGA/DSCi instrument which heat the sample from room temperature to 1000 ºC (10 ºC/min) in nitrogen atmosphere. Raman spectrums were obtained with a SENTERRA spectrometer using an excitation wavelength of 532 nm X-ray spectra analysis were developed by the diffractometer PHILIPS, PW-1711 with CuKα radiation ($\lambda = 0.15404$ nm). The following crystallographic parameters were studied: crystal stack height (Lc), interlaminar space (d) and the in-plane crystallite size or layer size (L_a).

$$d = \frac{\lambda}{2 \cdot sen\theta_1} \; ; \; L_c = \frac{k_1 \cdot \lambda}{FWHM \cdot cos\theta_1} \; ; \; L_a = \frac{k_2 \cdot \lambda}{FWHM \cdot cos\theta_2}$$

where:

- λ, radiation wavelength (λ = 0.15404 nm)
- θ_1, [002] or [001] diffraction peak position (º)
- θ_2, [100] diffraction peak position (º)
- k_1, form factor (k = 0.9)
- k_2, form factor (k = 1.84)
- FWHM, Full Width at Half Maximum of the corresponding diffraction peak (rad)

Electrochemical measurements were carried out in a single compartment electrochemical cell connected to an Autolab PGSTAT128N (Ecochemie, The Netherlands) Potentiostat/Galvanostat workstation. It is equipped with a Ag/AgCl (3 mol L^{-1} KCl, Metrohm®) as reference electrode, a Pt wire as counter electrode (Metrohm®) and a glassy carbon electrode, where carbonaceous materials are coated, as working electrode. 1 mol L^{-1} KCl aqueous solution was used as electrolyte in order to study the capacitive behavior of the synthetized materials. To this aim cyclic voltammetry studies were conducted at room temperature in the potential range from -1.0 V to +1.0 V at various scan rates (50, 100, 200 and 500 mV s^{-1}). The specific capacitance (C_s) of the samples was calculated using equation (1):

$$C_S(F \cdot g^{-1}) = \frac{I \cdot \Delta t}{m \cdot \Delta v} \qquad \text{(Eq. 1)}$$

where I is the constant current (A), $\Delta V/\Delta t$ is calculated from the discharge curve and m is the mass of active materials coated on the electrode as reported elsewhere [21] Prior to all tests, N_2 gas was bubbled for at least 20 min to remove the excess of oxygen solved in the electrolyte and flowed over the electrolyte during the cyclic voltammetry experiments. The ORR activity of the carbon-based materials was characterized by Linear sweep voltammetry by rotating disc electrode measurements at a scan rate of 10 mV s^{-1} in 0.1 mol L^{-1} KOH in an O_2 saturate solution. Rotation rate was varied from 200 to 2000 rpm. The chronoamperometry was developed at 1200 rpm during 10 hours in ^{1} in 0.1 mol L^{-1} KOH at a set potential of -1.297V in an O_2 saturate solution.

Finally, the point of zero charge (pH_{PZC}) value related to each synthetized material was determined with a Malvern Zetasizer Nano HT coupled with a MPT-2 titrator (Multi-purpose titrator) and a vacuum degasser. The suspension is placed in a cuvette screwed to the titrator MPT-2 associated to a pH meter. The sample is continuously agitated by a magnetic stirrer. In order to adjust the pH, 3 buckets are placed with different acid and base solutions, which are added to the suspension by means of 3 piston dosing pumps. 1 M NaOH, 0.25 M NaOH and 0.5 M HCl were used as titrating agents. Once the pH of the suspension is adjusted, it is pumped to the capillary cell located in the Zetasizer Nano equipment by means of a peristaltic roller pump, where the Zeta potential is measured. The pH sweep was registered from pH 10 to pH 2, at one pH unit intervals, at 25 °C. For each point, 3 repetitions of the Z-potential measurements were performed.

3. RESULTS

The surface chemical composition of GO, HT-rGO and rGO-PPy samples was analyzed by XPS. All samples showed C, O and N elements in the spectrum (see Table 1). The C/O ratio markedly increase after the different GO treatments indicating that most of the oxygen functionalities have been removed of the GO structure. Note that, C/O ratios were lower in rGO-PPy samples compared to HT-rGO.

Table 1: Elemental analysis of the materials

Material	C (%)	N (%)	O (%)	C/O
GO	51	0	49	1.04
HT-rGO	83	1	15	5.53
rGO-PPy450	74	8	18	4.11
rGO-PPy700	73	6	21	3.47

Table 2 shows the XPS N1s core level spectra fitting for rGO-PPy samples (N content of the HT-rGO sample was so low that, it was impossible to performance the N1s peak treatment because the XPS equipment does not have enough sensitivity to detect it) showing its decomposition in three peaks: pyrrolic N (398.2 eV) or N bonded to two C atoms with two p-electrons localized in the π-conjugated system, pyridinic N (400.2 eV) bonded to two C atoms with one p-electron localized in the π-conjugated system and, quaternary/graphitic N (402 eV) in with N substitutes a C atom in the hexagonal ring [22].

It is worthwhile to note the formation of appreciable amount of pyridinic N in both samples, which would be favorable for electrochemical properties of the materials [23]. Moreover, with an increase in the annealing temperature, the total and pyrrolic N decrease while the pyridinic N lightly increases. By its part, the C1s core level spectra fitting for GO sample (Table 2) could be decomposed into four Gaussian peaks at around 284.4 eV (C-C or sp^2 component), 286.5 eV (C-O), 288 eV (C=O) and, 289.2 eV (O-C=O). After hydrothermal reduction, peaks related to C-O, C=O and O-C=O remarkably decreased indicating the high reduction degree of GO [24, 25]. The same behavior was observed in rGO-PPy samples, but in this case, the decrease is less pronounced. Moreover, an additional component attributed to C-N bonds appeared at 285.7 eV in rGO-PPy samples [26]. The (π-π*) graphitic shakeup satellite contribution, noticed around ~291 eV, evolves upon reduction of GO. This implies the delocalized π conjugation, a conventional trait of the aromatic carbon structure, was to some degree restored in reduced GO [27]. It is important to highlight how, the sp^2 fraction of GO of around 65%, increases in HT-RGO sample to 83% Csp^2 which is indicative of a better ordered structure as a consequence of the restoration of the graphitic structure upon removal of O functionalities. Nevertheless, Csp^2 considerably decreases in the GO-PPy samples indicating the loss of graphitic nature of these samples.

Table 22 N1s and C1s XPS analysis spectra fitting

	XPS (N1s)			**XPS (C1s)**					
Material	**Pyridinic N (%)**	**Pyrrolic N (%)**	**Quaternary N (%)**	**-C-C- (%)**	**-C-N (%)**	**-C-O (%)**	**-C=O (%)**	**O-C=O (%)**	**π→π* (%)**
GO	-	-	-	65	-	20	11	4	-
HT-rGO	-	-	-	83	-	9	4	2	2
rGO-PPy450	39	55	6	49	26	13	6	4	2
rGO-PPy700	42	52	6	54	24	12	4	3	2

FTIR spectra of GO and the reduced-GO materials are displayed in Figure 1 in order to investigate their chemical structure.

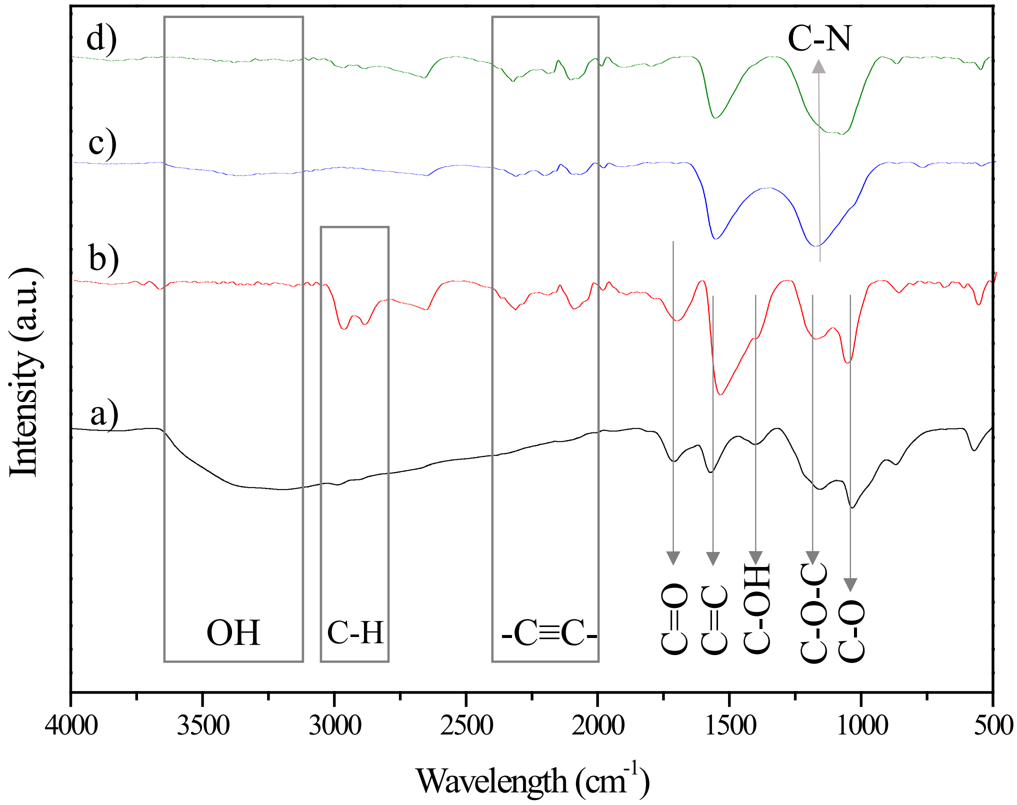

Figure 1: FTIR materials spectra a) GO; b) HT-rGO; c) rGO-PPy450; d) rGO-PPy700

Several functional groups are observed in GO structure: the most intense peak, attributed to the O-H stretching vibrations of a hydroxyl group and water molecules, occurs in the range 3000-3600 cm^{-1} being also observed the, deformation vibration modes of OH groups around 1430 cm^{-1}; band located at 2890 cm^{-1} correspond to alkene groups (C – H); band appearing at around 1710-1760 cm^{-1} is attributed to the C=O stretching vibration of a carbonyl group; band located at approximately 1630 cm^{-1} is attributed to the C=C skeletal vibration of the graphene planes; peak appearing at 1220-1230 cm^{-1} has been attributed to the stretching vibration of epoxy C-O-C group and, band at around 1050-1100 cm^{-1} is attributed to the alkoxy C-O stretching vibration (carboxyl group).

The hydrothermal reduction process of GO involves the removal of an important part of these oxygen functional groups. FT-IR spectra of HT-rGO sample displays that most of the hydroxyl groups are removed while, the other oxygen groups are only partially removed, showing a FTIR spectrum with the presence of the characteristic peaks of certain functional groups already commented for GO [28]. It is clearly observed how, the peak corresponding to the C=C vibration of the carbonaceous skeleton is intensified after hydrothermal reduction which corroborate XPS results.

FTIR spectra associated to the rGO-PPy samples clearly confirm the partial reduction of the oxygen functional groups after the treatment, implying that the oxygen functional groups have been converted into N-doped carbon through the carbonization of PPy [23]. Thus, two broad bands between 900-1750 cm^{-1} appear due to the overlapping of different peaks. Broad band appearing at 900-1375 cm^{-1} includes, apart from the remaining oxygenated groups already commented, the characteristic vibration peak of the C-N in plane deformation due to the doped bands at around 1220 cm^{-1}. Band between 1375-1750 cm^{-1} includes the characteristic PPy peaks at 1580 and 1450 cm^{-1} which are still important after annealing at 450º C although less at 700 ºC, indicating the presence of (non-carbonized) PPy in the GO-PPy samples [29]. Irregular peaks appearing around 2050-2400 cm^{-1} in all reduced samples could be attributed to –C≡C– stretch.

Figure 2 shows the RAMAN spectrums of the different samples. As observed, all samples showed spectra with two peaks centered at 1350 cm^{-1} (D band caused by edge imperfections) and, at 1590 cm^{-1} (G band, attributed to the vibration of sp2-bonded carbon atoms in a two-dimensional hexagonal lattice). The intensity ratio of D and G band, which can be used to monitored local defects, was higher in the reduced samples indicating their higher distortion [30]. Clearly, both D and G bands broadened after PPy polymerization on GO surface and subsequent annealing, suggesting that the size of the graphene oxide nanocrystals decreases [23]. This fact is much less marked in HT-rGO sample indicating that the GO particles does not experience such a drastic change. Additionally, after oxygen functionalities reduction, G peak position shifted to lower values (from 1593 cm^{-1} in GO to 1585 cm^{-1} in HT-rGO and, 1570-1578 cm^{-1} in rGO-PPy samples) which, as was confirmed by XPS, indicated a lower size of the sp^2 domains in these samples probably due to the π-π interactions (stronger in the case of π-π interactions between GO and PPy). Characteristic vibrational peaks of PPy (Figure 2, inset [14]) are clearly evident in the rGO-PPy nanocomposite RAMAN spectrum, leading to the disappearance of the characteristic form of the (D and G) GO bands. Thus, C=C backbone stretching and, ring-stretching mode RAMAN bands associated at PPy at 1317 and 1550 cm^{-1}, respectively, overlap with D and G band of graphene oxide [31]. Results indicate that PPy and GO are not simply blended or mixed up, existing a strong interaction between remaining PPy and GO.

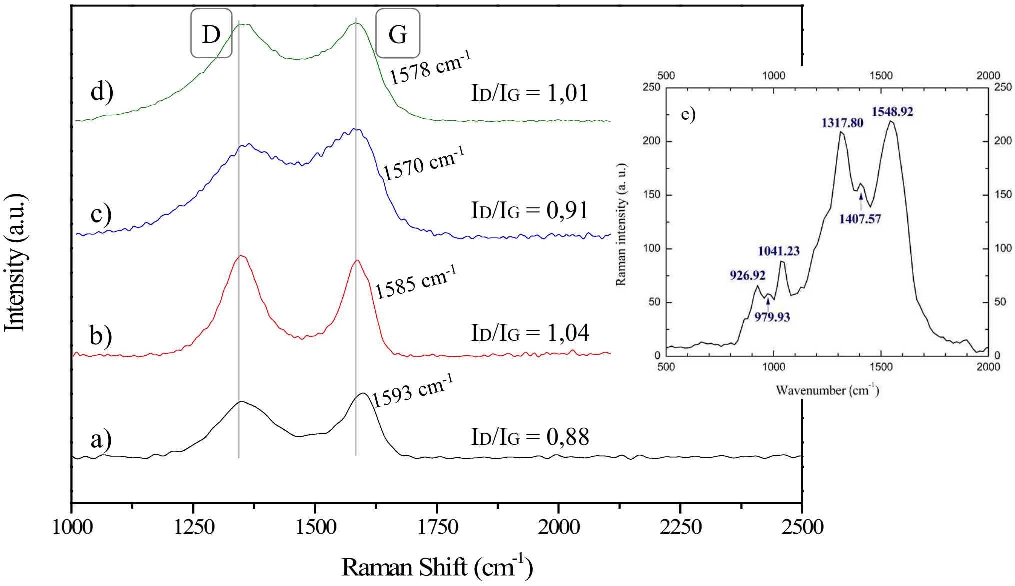

Figure 2: Raman materials spectra. a) GO; b) HT-rGO; c) rGO-PPy450; d) rGO-PPy700; e) PPy [32]

X-ray diffraction analysis was used to measure crystal structures. Figure 3 presents the XRD patterns and Table 3, the main crystallographic parameters of GO, HT-rGO and rGO-PPy samples. The synthesized GO exhibits the (001) peak at $2\Theta \approx 9.3^{o}$ as reported in existing literature [33] which indicates the formation of layer-like GO sheets with a interplanar spacing of 0.94 nm (comparing to natural graphite, (001) peak appears after graphite oxidation, while, intense (002) peak characteristic of graphite, disappears). The diffraction peak at around 43^{o} is associated with the (100) plane of the hexagonal structure of carbon [33]. For the rGO-PPy composite structure, the (001) reflection peak of GO disappears and, a broad (002) diffraction peak appear between $25.8\text{-}26.3^{o}$ indicating the formation of short range ordered stacks in rGO-PPy samples (higher level of defects) [25]. As observed in Table 3, $\mathrm{FWHM}_{(002)}$ value decreases at high annealing temperature as a consequence of high level of carbonization of the amorphous PPy in sample rGO-PPy700 (although polymer is not completely carbonized). From crystallographic parameters showed in Table 3, it can be found that HT-rGO sample restacked into a much more ordered crystalline structure [34] compared to the rGO-PPy samples. Thus, although L_a values are almost the same, L_c values considerably decrease after PPy treatment which is in agreement with RAMAN results. Furthermore, the smaller peak at 43^{o} in reduced samples (compared to the GO base) confirms the removal of oxygen functional groups of the GO sheets [34].

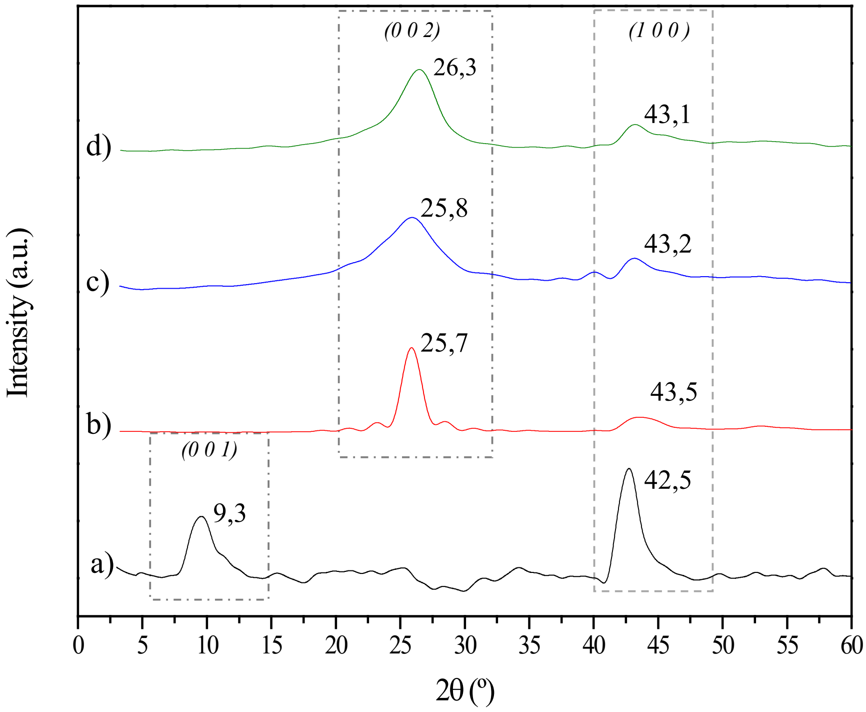

Figure 3: X-ray diffractograms. a) GO; b) HT-rGO; c) rGO-PPy450; d) rGO-PPy700

Table 3: XRD crystallographic parameters

Material	FWHM$_{002}$	L$_a$ (nm)	L$_c$ (nm)	d (nm)
GO	-	8.9	8.2	0.94
HT-rGO	1.6	5.4	5.0	0.35
rGO-PPy450	4.7	5.9	1.7	0.34
rGO-PPy700	3.4	5.1	2.4	0.34

FWHM: Full width at half-maximum corresponding to diffraction peak
d: interlayer distance obtained by XRD.
L_c, L_a: medium crystallite layer size obtained by XRD

Figure 4 shows thermogravimetric analysis results corresponding to GO and rGO-PPy samples. GO showed a TGA curve in which three different weight loss steps could be differentiated. The first one (I), appearing between 0 and 200°C, was mainly due to the removal of both water solvent molecules and, to the thermally induced decomposition of the more labile oxygen functional groups and subsequent release of steam and gases (CO, CO_2) losing around 37% of mass. The second weight loss step (II), occurring between

200 and 500ºC approximately, was due to the removal of the more thermally stable oxygen groups with a weigh loss of around 18% of the total mass. Finally, a third step (III) for temperatures above 500ºC, was observed as a consequence of the material thermal degradation, losing around 38% of the remaining mass at 1000ºC. Removal of oxygenated functional groups is mainly due to the CO and CO_2 evolution involving the generation of atomic vacancies and voids into the structure [35]. The low temperature elimination (<200ºC) of an important part of the oxygen functional groups present in the GO structure, is favored by the high oxygen density in GO [36].

On the other hand, a huge thermal stability improvement was observed for the GO-PPy samples compared to GO base. Moreover, annealing temperature clearly influence over the thermal stability. Thus, weight loss around 200ºC is mainly due to the removal of the remaining oxygen containing functional groups in the samples. Major weight loss was observed in sample rGO-PPy450 than in rGO-PPy700 from 200 to 750ºC due to the decomposition of the remaining PPy in the former [37]. In general, the high thermal stability of the reduced samples compared to GO base is due to the removal of the major part of the structural oxygen functional groups, as can be also corroborated by the HT-rGO sample thermogravimetric analysis which showed the highest thermal stability with only a 11% of weight loss. Finally, weight loss between 750-1000ºC was similar for both rGO-PPy samples, losing around 7-9% of the remaining mass due to the combustion of the graphene to CO or CO_2.

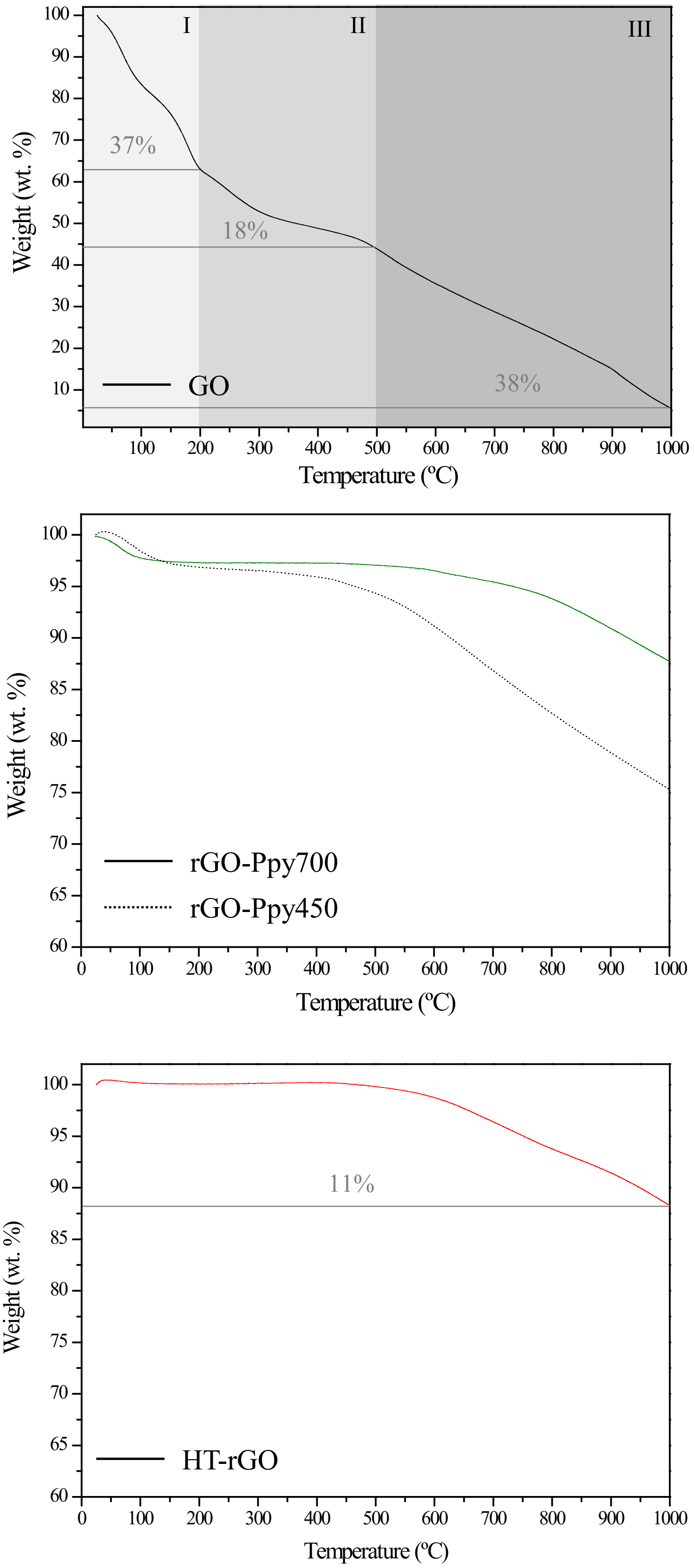

Figure 4: Thermogravimetric analysis for graphene-based materials.

The surface charge on the graphene-based nanomaterials (mV) was determined in solution and plotted against pH (Figure 5). Zeta potential essays is used to measure the surface properties and the stability in aqueous solution of the carbonaceous nanomaterials since, their surface charge could influence the electronic characteristics of the active phase in case for example, of being used the graphene-based materials as a catalyst support. If all the particles in suspension have a large negative or positive zeta potential (±30 mV) then, they will trend to repel each other and there is no tendency to accumulate. However, if the particles have low zeta potential values there is no force to prevent the particles come together and agglomerate. Thus, a larger Zeta potential means there has been a better dispersion of particles in the solution. The zero point charge (pH_{ZPC}) is defined as the pH at which the surface of the material has net electrical neutrality [38]. Commonly, the ZPC point is where the nanoscale and colloidal systems have at least stability and agglomeration was occurred, because of van der Waals force overcomes to electrostatic repulsion [39].

From results depicted in Figure 5, the presence of oxygen functionalities on GO contribute to the formation of acid sites in response to pH changes (mainly the ionization of the carboxylic acid groups). As the pH is increased, the surface charge become more negative, approximately −22 mV (at pH 2) to −30 mV (at pH-7). Accordingly, GO is negatively charged and zeta potential values were below − 30 mV from pH=3 due to more oxygen groups are ionized forming negatively charged radicals [40], which could be indicative of that GO have sufficient mutual repulsion force and form stable colloidal dispersion [41].

On the other hand, for all rGO samples, their zeta potential become more negative with increasing pH but, magnitude of zeta potentials are lower than that of GO at the same pH (until pH=7-8) as a consequence of the removal of the oxygen containing functional groups (lower concentration of the ionized groups). The point of zero charge (pH_{pzc}) of rGO-PPy700 and rGO-PPy450 takes place at pH of 3.8 and 4.3, respectively and at pH of 7.1 for sample HT-rGO which revealed a significant modification of the surface charge behavior with an increase of the surface basicity (as a function of the pH value) after oxygen functionalities reduction [42, 43, 44]. The higher pH_{pzc} of HT-rGO compared to rGO-PPy samples, may be due to its restack into a much more ordered crystalline structure.

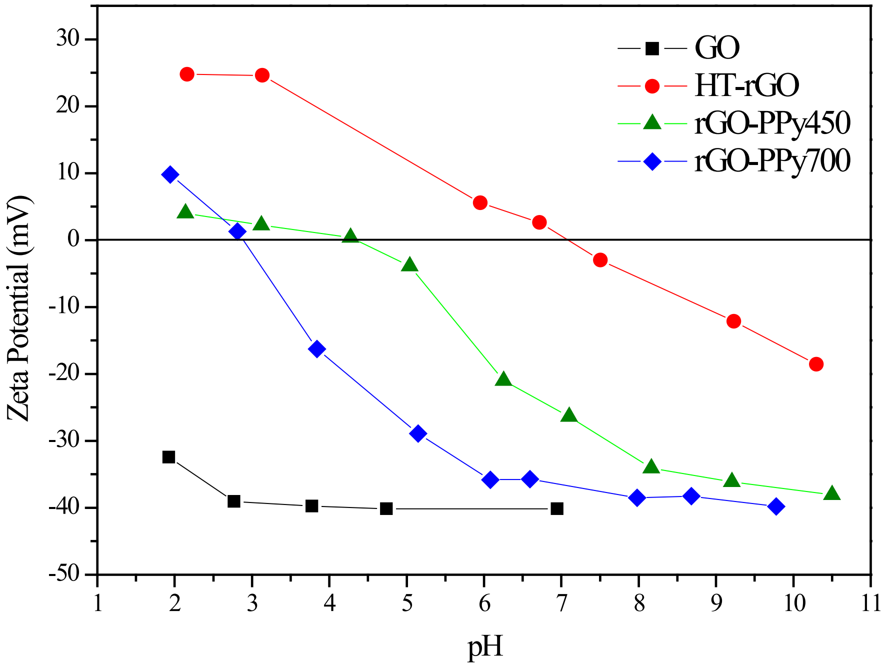

Figure 5: pH dependence of the surface charge of graphene-based materials

Regarding the capacitive behavior of graphene-based materials, it is well known that the corresponding electrochemical capacitance is mainly influenced by their surface area and pore structure. Voltammogram is often used to calculate the specific capacitance value of the electrode materials. Therefore, capacitance values (Cs) for all samples, expressed in Farads per gram, are calculated through Eq. 1, detailed in the characterization section, and listed in Table 4.

Table 4: Capacitance values at 50 $mV \cdot s^{-1}$, room temperature, 1 M KCl

Material	C (F/g)
GO	91.5
rGO-PPy450	86.9
rGO-PPy700	74.1
HT-rGO	60.0

The significant deviation in the quasi-rectangular shape of the CV curves (not shown here) signifies the pseudo-capacitance behavior of the samples due to its oxygen functionalities, which facilitate a faradaic redox reaction between the electrolyte ions and working electrode. In this sense, the areas of the CV curves corresponding to the GO sample were observed to be higher than those of rGO-PPy450, rGO-PPy 700 and HT-rGO samples, which indicates that GO exhibit higher specific capacitance than that of reduced-GO materials. The enhancement in the specific capacitance of GO might be due to the intrinsic higher porosity in conjunction with the synthesis procedure of the reduced materials, which favor the restacking of graphene sheets after reduction (see Figure 6 where the wrinkled GO sheets and the more development surface of GO compared to the reduced samples can be observed), leading to lower electrochemical resistance for ionic diffusion between the graphene sheets. It was also observed that the increase of the annealing reduction temperature causes a decrease in the specific capacitance of the rGO-PPy samples.

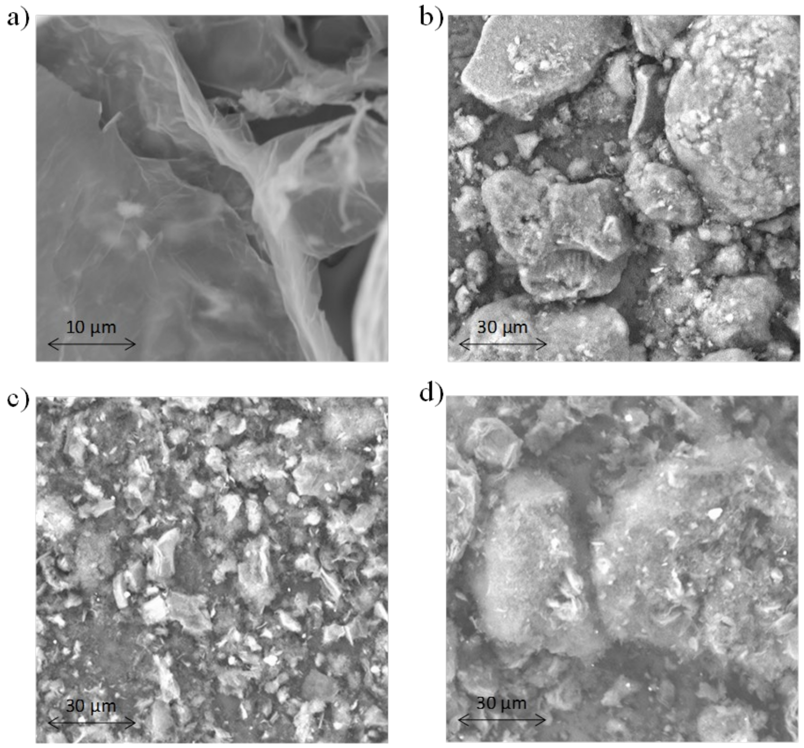

Figure 6: SEM images of a) GO, b) HT-rGO, c) rGO-PPy450, d) rGO-PPy700

Regarding ORR activity, it is known that the kinetics are controlled by the binding energies between the catalyst and oxygen containing intermediates (O_2^-, HO_2^-, and OH^-). Therefore, ORR can proceed by three feasible reaction pathways in alkaline media, depending on the stability of those intermediates generated after O_2 adsorption on the support sample: (i) direct 4-electron pathway to generate H_2O, (ii) two-electron pathway to produce HO_2^- and OH^- and (iii) indirect 2×2 electron pathway (HO_2^- intermediate). Note that pathways ii) and iii) cannot be considered completely independent since they are strongly influenced by the pH, the HO_2^- adsorption/desorption rate and the applied potential [45, 46, 47, 48].

It is clear from Figure 7a) that, rGO-PPy samples show higher electrocatalytic activity than parent GO in terms of current density, which shifts towards a more positive value attributed to the effect of the high amount of pyridinic N species. HT-rGO also shows the same trend showing higher current density values vs. GO. The onset potential (E_{onset}) is a key parameter for evaluate ORR activitiy of the materials. It can be observed again, that the hydrothermal reduction provide a slightly higher value of onset potential (E_{onset} = -0.022 V) than those of polypyrrole-based samples at 450 and 700ºC (E_{onset} = -0.014 V and E_{onset} = -0.015 V, respectively). Attending to this, nitrogen doped carbonaceous materials exhibit a less negative value than that of the GO raw material (E_{onset} = -0.16V).

Figure 7b) shows the Tafel obtained from the ORR polarization curves in order to explore the difference in kinetics on these metal-free carbonaceous materials. As can be observed in Tafel slopes at low current densities, the polypyrrole materials rGO-PPy450 and rGO-PPy700 exhibit a lower Tafel slopes (60.44 and 47.54mV·dec^{-1}) than the GO raw material (111.31 mV·dec^{-1}) and the reduced material HT-rGO (67.21 mV·dec^{-1}). This fact suggests the favorable ORR kinetics of the PPy samples due to the presence of nitrogen groups producing active sites where the ORR reaction takes place. Particularly, the best results are those obtained by the rGO-PPy700.

On the other hand, from Figure 8 and Table 6, which summarizes RDE data measurements, the electrons transferred calculated from the slope of the polarization curves were in the range between 2 and 4 (at -0.6 V), which reveals that ORR takes place in two steps. As expected, n value shifts to higher values while modifying potential from -0.4 V to -0.8 V (not shown). Hence, the obtained n values for GO and rGO-PPy samples were similar and close to four which shows an almost complete reaction pathway. Factors such as a high specific surface area, low level of graphene layers restacking and the presence of pyridinic N functionalities are found to promote the adsorption of oxygen, facilitating the formation of ORR intermediates and increasing the electron transferred, which improves the catalytic activity [7, 49, 50, 51]. On the other hand HT-rGO proceed with a lower number of electrons due to its restacked into a much more ordered crystalline structure. Hence, according to these results the Polypyrrole-reduced synthesis method seems to be the preferred one for the ORR application of graphene based materials. Particularly, the best results are those obtained by the rGO-PPy700. For that reason, it was studied the mild-term stability for this catalyst in order to corroborate the non-degradation of the chosen one.

The stability of the electrocatalyst is an important factor in the study of electrochemical characterization. Figure 9 shows the chronoamperometry test developed for the more suitable carbon material for ORR studied in this paper (rGO-PPy700). The stability test was conducted at applied potential of -1.297 V (vs RHE) for 10 hours. After the first two hours, the current density for the rGO-PPy700 has reached -3.0 mA, this value is close enough to the value obtained on the polarization curves in figure 7a). During the next hours there is no obvious change detected. This fact reflects a high durability of the carbonaceous material used as electrocatalyst in the ORR.

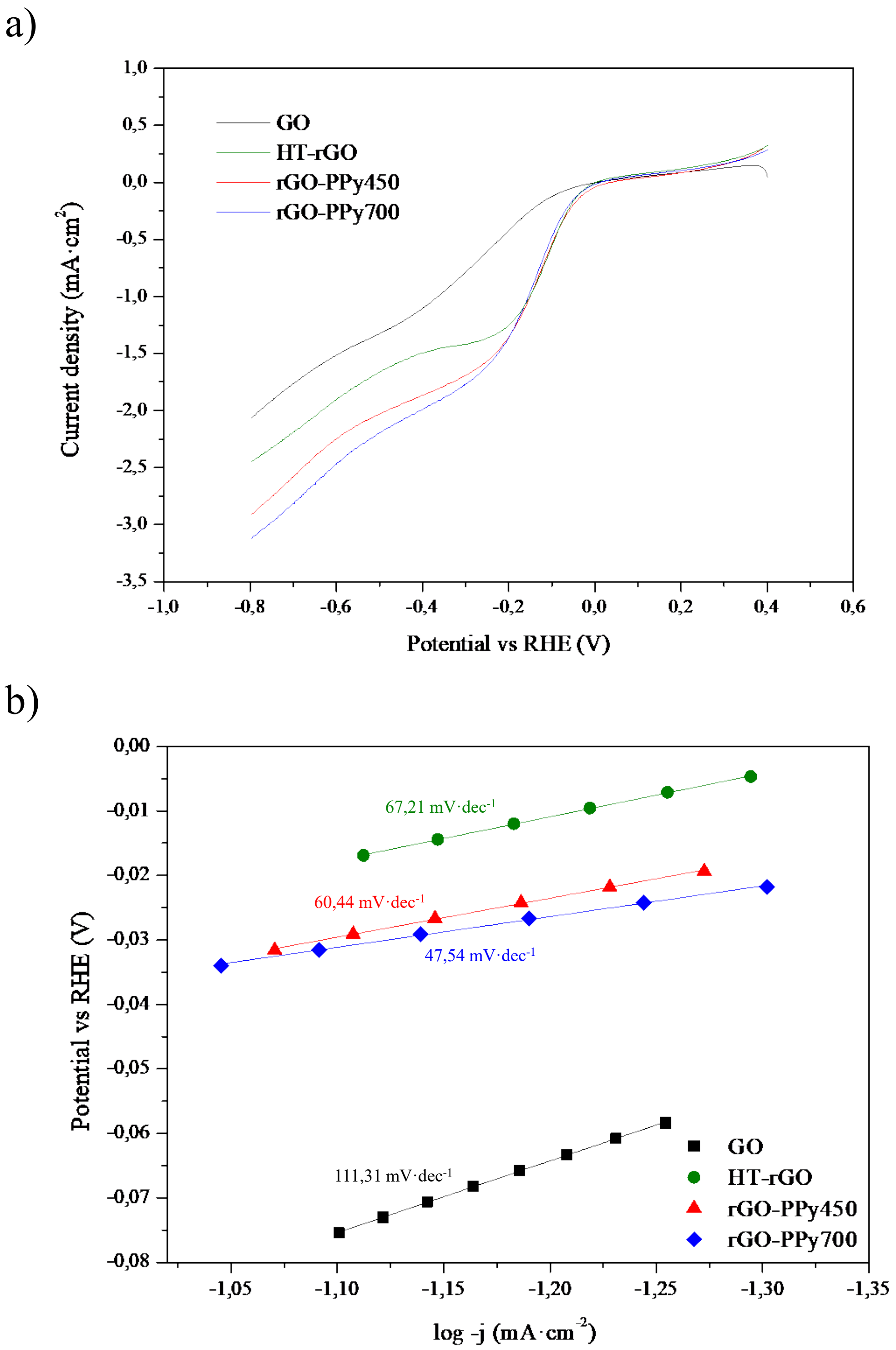

Figure 7. a) Comparative RDE polarization curves for ORR in O_2 saturated 0.1M KOH. Room temperature. Scan rate 10 mV·s^{-1}. b) Tafel plot for ORR.

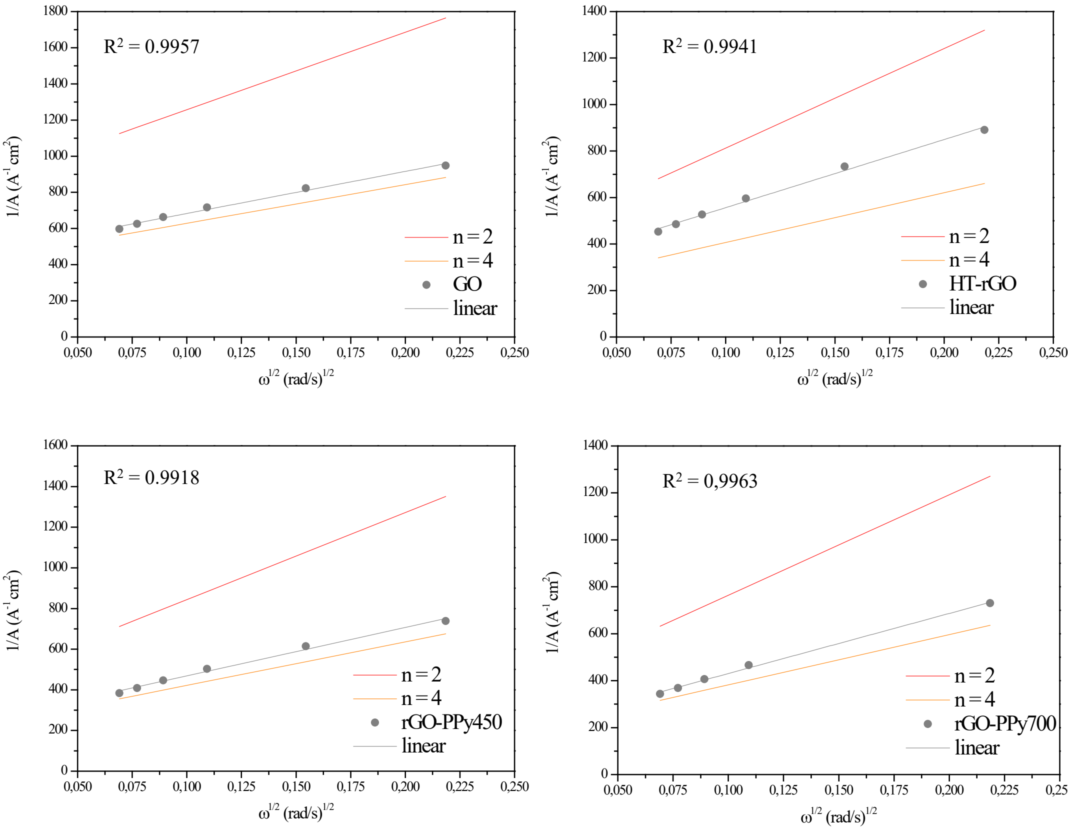

Figure 8. Koutecky-Levich plots derived from polarization curves recorded at different rotation rates at -0.6 V.

Table 6: ORR. Potential: -0.6 V; KOH 0.1 M; room temperature; Scan rate 10 mV·s^{-1}

Sample	Electrons transferred per O_2 molecule (n)
GO	3.6
rGO-PPy450	3.6
rGO-PPy700	3.7
HT-rGO	2.9

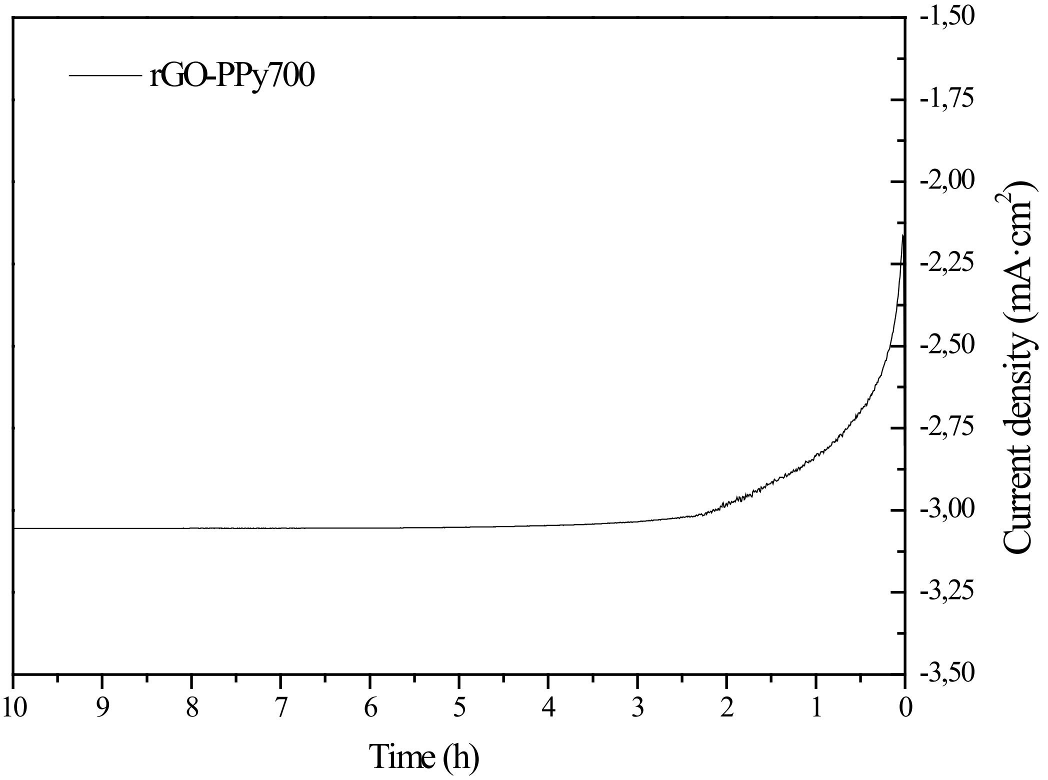

Figure 9. Chronoamperometry of the rGO-PPy700 measured at -1.297 V at 1200 rpm.

CONCLUSIONS

Two different approaches to simultaneously introduce nitrogen atoms within the graphene framework and, reduce graphene oxide nanoplatelets (GO), have been explored in order to improve the electrocatalytic activity of the resulting materials. Thus, a facile hydrothermal method using 2-chloroethylamine under conditions at 180 ºC and, another one, based in the formation of polypyrrole (PPy) on graphene oxide nanoplatelets by in situ polymerization of pyrrole monomer in the presence of GO, were compared through a deep characterization of the final materials. Physico-chemical properties of the graphene-based materials were subsequently related with their electron transfer efficiency and electrocatalytic activity. The as prepared PPy-rGO materials showed an N content quite superior (6-8 %) to the rGO prepared by the hydrothermal method (1%) being an important part of their nitrogen state pyridinic type. After the two different reduction treatments, GO experimented an important restacking of the graphene sheets which lead to a lower electrochemical resistance for ionic diffusion between the graphene sheets. In relation to that, GO exhibited high specific capacitance than that of reduced-GO materials due to its intrinsic higher porosity. On the other hand, the presence of N species seems to have a positive effect on the ORR activity however, the N incorporation through the PPy-rGO synthesis method seems to be the preferred one according for the complete ORR pathway.

Acknowledgment

The authors acknowledge financial support from the Spanish company Graphenano Nanotechnologies UCTR16017.

The authors acknowledge Inorganic Chemistry Department of the University of Cordoba for the XPS spectroscopy measures.

REFERENCES

[1] L.M. Rivera, G. García, E. Pastor, Novel graphene materials for the oxygen reduction reaction, Curr. Opin. Electrochem., 9 (2018) 233-239.
[2] Z. Lu, G. Chen, S. Siahrostami, Z. Chen, K. Liu, J. Xie, L. Liao, T. Wu, D. Lin, Y. Liu, T.F. Jaramillo, J.K. Nørskov, Y. Cui, High-efficiency oxygen reduction to hydrogen peroxide catalysed by oxidized carbon materials, Nature Catalysis, 1 (2018) 156-162.
[3] Q. Xiang, S. Li, X. Zou, Y. Qiang, B. Hu, Y. Cen, C. Xu, L. Liu, Y. Zhou, C. Chen, Self-assembly porous metal-free electrocatalysts templated from sulfur for efficient oxygen reduction reaction, Appl. Surf. Sci., 462 (2018) 65-72.
[4] J. Zhang, L. Dai, Heteroatom-Doped Graphitic Carbon Catalysts for Efficient Electrocatalysis of Oxygen Reduction Reaction, ACS Catalysis, 5 (2015) 7244-7253.
[5] H.-J. Niu, L. Zhang, J.-J. Feng, Q.-L. Zhang, H. Huang, A.-J. Wang, Graphene-encapsulated cobalt nanoparticles embedded in porous nitrogen-doped graphitic carbon nanosheets as efficient electrocatalysts for oxygen reduction reaction, J. Colloid Interface Sci., 552 (2019) 744-751.
[6] T. Ikeda, M. Boero, S.-F. Huang, K. Terakura, M. Oshima, J.-i. Ozaki, Carbon Alloy Catalysts: Active Sites for Oxygen Reduction Reaction, J Phys Chem C, 112 (2008) 14706-14709.

[7] Z. Lin, G.H. Waller, Y. Liu, M. Liu, C.-p. Wong, 3D Nitrogen-doped graphene prepared by pyrolysis of graphene oxide with polypyrrole for electrocatalysis of oxygen reduction reaction, Nano Energy, 2 (2013) 241-248.
[8] J. Vazquez-Arenas, A. Galano, D.U. Lee, D. Higgins, A. Guevara-García, Z. Chen, Theoretical and experimental studies of highly active graphene nanosheets to determine catalytic nitrogen sites responsible for the oxygen reduction reaction in alkaline media, J. Mater. Chem. A., 4 (2016) 976-990.
[9] Q. Xiang, Y. Liu, X. Zou, B. Hu, Y. Qiang, D. Yu, W. Yin, C. Chen, Hydrothermal Synthesis of a New Kind of N-Doped Graphene Gel-like Hybrid As an Enhanced ORR Electrocatalyst, ACS Applied Materials & Interfaces, 10 (2018) 10842-10850.
[10] M. Sun, X. Wu, Z. Xie, X. Deng, J. Wen, Q. Huang, B. Huang, Tailoring platelet carbon nanofibers for high-purity Pyridinic-N doping: A novel method for synthesizing oxygen reduction reaction catalysts, Carbon, 125 (2017) 401-408.
[11] H. Zhang, Y. Wang, D. Wang, Y. Li, X. Liu, P. Liu, H. Yang, T. An, Z. Tang, H. Zhao, Hydrothermal Transformation of Dried Grass into Graphitic Carbon-Based High Performance Electrocatalyst for Oxygen Reduction Reaction, Small, 10 (2014) 3371-3378.
[12] C. Zhang, R. Hao, H. Liao, Y. Hou, Synthesis of amino-functionalized graphene as metal-free catalyst and exploration of the roles of various nitrogen states in oxygen reduction reaction, Nano Energy, 2 (2013) 88-97.
[13] N.-W. Pu, C.-Y. Chen, H.-X. Qiu, Y.-M. Liu, C.-H. Song, M.-H. Lin, M.-D. Ger, Hydrothermal Synthesis of N-Doped Graphene/Fe2O3 Nanocomposite for Supercapacitors, Int. J. Electrohcem. Sc., 13 (2018) 6812-6823.
[14] M. Mehmood Shahid, A.H. Ismail, A.M.A.A.A. Al-Mokaram, R. Vikneswaran, S. Ahmad, A. Hamza, A. Numan, A single-step synthesis of nitrogen-doped graphene sheets decorated with cobalt hydroxide nanoflakes for the determination of dopamine, Prog. Nat. Sci. Mater., 27 (2017) 582-587.
[15] Z. Jiang, X. Zhao, X. Tian, L. Luo, J. Fang, H. Gao, Z.-J. Jiang, Hydrothermal Synthesis of Boron and Nitrogen Codoped Hollow Graphene Microspheres with Enhanced Electrocatalytic Activity for Oxygen Reduction Reaction, ACS Applied Materials & Interfaces, 7 (2015) 19398-19407.
[16] K. Zhang, L.L. Zhang, X.S. Zhao, J. Wu, Graphene/Polyaniline Nanofiber Composites as Supercapacitor Electrodes, Chem. Mater., 22 (2010) 1392-1401.
[17] K. Lee, L. Zhang, H. Lui, R. Hui, Z. Shi, J. Zhang, Oxygen reduction reaction (ORR) catalyzed by carbon-supported cobalt polypyrrole (Co-PPy/C) electrocatalysts, Electrochim. Acta, 54 (2009) 4704-4711.
[18] M.d.P. Lavin-Lopez, A. Romero, J. Garrido, L. Sanchez-Silva, J.L. Valverde, Influence of Different Improved Hummers Method Modifications on the Characteristics of Graphite Oxide in Order to Make a More Easily Scalable Method, Ind. Eng. Chem. Res., 55 (2016) 12836-12847.
[19] A. Ariharan, B. Viswanathan, V. Nandhakumar, Nitrogen doped graphene as potential material for hydrogen storage, Graphene, 6 (2017) 41.
[20] L.F. Chen, X.D. Zhang, H.W. Liang, M. Kong, Q.F. Guan, P. Chen, Z.Y. Wu, S.H. Yu, Synthesis of nitrogen-doped porous carbon nanofibers as an efficient electrode material for supercapacitors, ACS nano, 6 (2012) 7092-7102.
[21] A. Ramesh, M. Jeyavelan, M.S. Leo Hudson, Electrochemical properties of reduced graphene oxide derived through camphor assisted combustion of graphite oxide, Dalton T., 47 (2018) 5406-5414.
[22] E.P. Randviir, D.A. Brownson, C.E. Banks, A decade of graphene research: production, applications and outlook, Mater. Today, 17 (2014) 426-432.
[23] S.K. Srivastava, J. Pionteck, Recent advances in preparation, structure, properties and applications of graphite oxide, J Nanosci Nanotechno, 15 (2015) 1984-2000.
[24] Q.A. Khan, A. Shaur, T.A. Khan, Y.F. Joya, M. Awan, Characterization of reduced graphene oxide produced through a modified Hoffman method, Cogent. Chem., 3 (2017) 1298980.

[25] L. Samiee, A. Yadegari, S. Tasharrofi, One-Pot Facile Synthesis of N-Doped Graphene Synthesized from Paraphenylenediamine as Metal-Free Catalysts for the Oxygen Reduction Used for Alkaline Fuel Cells, International Journal of Chemical, Molecular, Nuclear, Materials and Metallurgical Engineering, 10 (2016) 510-514.
[26] C. Simón-Herrero, S. Caminero-Huertas, A. Romero, J.L. Valverde, L. Sánchez-Silva, Effects of freeze-drying conditions on aerogel properties, J. Mater. Sci., 51 (2016) 8977-8985.
[27] W. Gao, L.B. Alemany, L. Ci, P.M. Ajayan, New insights into the structure and reduction of graphite oxide, Nature chemistry, 1 (2009) 403.
[28] L.G. Cançado, A. Jorio, E.M. Ferreira, F. Stavale, C. Achete, R. Capaz, M. Moutinho, A. Lombardo, T. Kulmala, A.C. Ferrari, Quantifying defects in graphene via Raman spectroscopy at different excitation energies, Nano Lett., 11 (2011) 3190-3196.
[29] J. Kotakoski, A. Krasheninnikov, U. Kaiser, J. Meyer, From point defects in graphene to two-dimensional amorphous carbon, Phys. Rev. Lett., 106 (2011) 105505.
[30] A. Jorio, E. Kauppinen, A. Hassanien, Carbon-nanotube metrology, Carbon Nanotubes, 111 (2008) 63-100.
[31] L. Panchakarla, K. Subrahmanyam, S. Saha, A. Govindaraj, H. Krishnamurthy, U. Waghmare, C. Rao, Synthesis, structure, and properties of boron-and nitrogen-doped graphene, Adv. Mater., 21 (2009) 4726-4730.
[32] P. Herrera Herrera, N. Casillas Santana, J. Aguilar Martinez, Electrosynthesis and DSC Characterization of Doped Polypyrrole Films with Sodium Salicylate and Sodium Ibuprofen on the Mg Alloy AZ31, ECS Transactions, 84 (2018) 243-256.
[33] M.d.P. Lavin-Lopez, A. Romero, J. Garrido, L. Sanchez-Silva, J.L. Valverde, Influence of Different Improved Hummers Method Modifications on the Characteristics of Graphite Oxide in Order to Make a More Easily Scalable Method, Ind. Eng. Chem. Res., 55 (2016) 12836-12847.
[34] M. Terrones, A. Souza Filho, A. Rao, Doped Carbon Nanotubes: Synthesis, Characterization and Applications Vol. 111, 531–566, Springer Topics in Appl. Phys., Springer, 2008.
[35] A. Romero, M. Lavin-Lopez, L. Sanchez-Silva, J. Valverde, A. Paton-Carrero, Comparative study of different scalable routes to synthesize graphene oxide and reduced graphene oxide, Mater. Chem. Phys., 203 (2018) 284-292.
[36] T. Sun, S. Fabris, S. Baroni, Surface precursors and reaction mechanisms for the thermal reduction of graphene basal surfaces oxidized by atomic oxygen, J. Phys. Chem. C, 115 (2011) 4730-4737.
[37] L. Panchakarla, A. Govindaraj, C. Rao, Nitrogen-and boron-doped double-walled carbon nanotubes, ACS nano, 1 (2007) 494-500.
[38] H. Xiao, H. Peng, S. Deng, X. Yang, Y. Zhang, Y. Li, Preparation of activated carbon from edible fungi residue by microwave assisted K2CO3 activation—Application in reactive black 5 adsorption from aqueous solution, Bioresour. Technol., 111 (2012) 127-133.
[39] M. Bahreini, M. Movahedi, M. Peyvandi, F. Nematollahi, H.S. Tehrani, Correlation Assessment of Zeta Potential and Catalytic Activity of Graphene Nano Sheets as Nanozyme, Eurasian J. Anal. Chem., 13 (2018).
[40] M.J. Li, C.M. Liu, Y.B. Xie, H.B. Cao, H. Zhao, Y. Zhang, The evolution of surface charge on graphene oxide during the reduction and its application in electroanalysis, Carbon, 66 (2014) 302-311.
[41] F. Baskoro, C.-B. Wong, S.R. Kumar, C.-W. Chang, C.-H. Chen, D.W. Chen, S.J. Lue, Graphene oxide-cation interaction: Inter-layer spacing and zeta potential changes in response to various salt solutions, J. Membr. Sci., 554 (2018) 253-263.
[42] A.H. Labulo, B. Omondi, V.O. Nyamori, Graphene/pyrrolic-structured nitrogen-doped CNT nanocomposite supports for Pd-catalysed Heck coupling and chemoselective hydrogenation of nitroarenes, SN Applied Sciences, 1 (2019) 142.
[43] C.K. Najeeb, J.H. Lee, J. Chang, J.H. Kim, The effect of surface modifications of carbon nanotubes on the electrical properties of inkjet-printed SWNT/PEDOT–PSS composite line patterns, Nanotechnology, 21 (2010) 385302.

[44] J. Amadou, K. Chizari, M. Houllé, I. Janowska, O. Ersen, D. Bégin, C. Pham-Huu, N-doped carbon nanotubes for liquid-phase CC bond hydrogenation, Catal. Today, 138 (2008) 62-68.
[45] F.H.B. Lima, M.L. Calegaro, E.A. Ticianelli, Electrocatalytic activity of manganese oxides prepared by thermal decomposition for oxygen reduction, Electrochim. Acta, 52 (2007) 3732-3738.
[46] J. Guo, A. Hsu, D. Chu, R. Chen, Improving Oxygen Reduction Reaction Activities on Carbon-Supported Ag Nanoparticles in Alkaline Solutions, J Phys Chem C, 114 (2010) 4324-4330.
[47] F. Cheng, J. Chen, Metal–air batteries: from oxygen reduction electrochemistry to cathode catalysts, Chem. Soc. Rev., 41 (2012) 2172-2192.
[48] X. Ge, A. Sumboja, D. Wuu, T. An, B. Li, F.W.T. Goh, T.S.A. Hor, Y. Zong, Z. Liu, Oxygen Reduction in Alkaline Media: From Mechanisms to Recent Advances of Catalysts, ACS Catalysis, 5 (2015) 4643-4667.
[49] L. Fu, Y. Zheng, P. Zhang, J. Zhu, H. Zhang, L. Zhang, W. Su, Embedding leaf tissue in graphene ink to improve signals in electrochemistry-based chemotaxonomy, Electrochem. Commun., 92 (2018) 39-42.
[50] L. Lai, J.R. Potts, D. Zhan, L. Wang, C.K. Poh, C. Tang, H. Gong, Z. Shen, J. Lin, R.S. Ruoff, Exploration of the active center structure of nitrogen-doped graphene-based catalysts for oxygen reduction reaction, Energy Environ. Sci., 5 (2012) 7936-7942.
[51] K.F. Babu, B. Rajagopalan, J.S. Chung, W.M. Choi, Facile synthesis of graphene/N-doped carbon nanowire composites as an effective electrocatalyst for the oxygen reduction reaction, Int. J. Hydrogen Energy, 40 (2015) 6827-6834.